# Floating Shock Fitting for Cones at Large Incidence

James Daywitt,* Paul Kutler,† and Dale Anderson‡
*Iowa State University, Ames, Iowa*
*and*
*NASA Ames Research Center, Moffett Field, Calif.*

**The technique of floating shock fitting is adapted to the computation of the inviscid flowfield about circular cones in a supersonic freestream at angles of attack that exceed the cone half-angle. In those regions in which the governing conical equations are mixed elliptic-hyperbolic, the fully hyperbolic form is obtained by the addition of the temporal derivative. For cones of infinite extent, the flow maintains its conical nature up to the detachment point. Thus, the resulting equations are applicable over the complete range of freestream Mach numbers, angles of attack, and cone half-angles for which the bow shock is attached. An explicit finite-difference algorithm is used to obtain the solution by an unsteady relaxation approach. The bow shock, embedded crossflow shock, and vortical singularity in the leeward symmetry plane are all treated as floating discontinuities in a fixed computational mesh. The method yields excellent results for the bow and embedded shocks; however, the solution in the leeward symmetry plane exhibits viscous-like effects and does not appear to adequately predict the behavior of the vortical singularity.**

## Introduction

MANY numerical methods (Ref. 1 contains a representative list), that have been successfully applied to the computation of the inviscid flowfield about sharp circular cones at incidence to a supersonic freestream are limited to cases where the angle of attack $\alpha$ does not greatly exceed the cone half-angle $\theta_c$ ($\alpha/\theta_c \lesssim 1$) or are restricted to solving only the windward portion of the flowfield. The numerical difficulties associated with large relative angles of attack $\alpha/\theta_c$ are attributable to the appearance of new flow features on the leeward side of the cone.

At moderate angles of attack, the crossflow velocity (the projection of the velocity vector onto the surface of a unit sphere centered at the cone apex) is everywhere subsonic. At large incidence, the crossflow accelerates from the windward symmetry plane to supersonic velocities in the shoulder region of the cone. To satisfy the leeward symmetry plane boundary conditions, an embedded conical crossflow shock (not present at smaller angles of attack) forms to decelerate the crossflow (Fig. 1).

The assumptions of conical and inviscid flow result in the appearance of a vortical singularity,[2] i.e., a nodal singularity, conical stagnation point at which the entropy, density, and radial velocity component $u$ are multivalued. The nature of this singularity for cones at large angles of attack has been investigated in several theoretical and numerical studies,[2-7] and an analogous feature has even been found in some experimental results.[8,9] The theoretical predictions for the behavior of the vortical singularity are based upon linear theory or localized solutions and thus cannot account for the effects of the crossflow shock. However, the conjecture that the vortical singularity will, at large angles of attack, lift off the cone surface in the leeward symmetry plane has been supported by numerical methods.[5-7]

Explicit finite-difference techniques[5,10,11] provided the first evidence for the inviscid, nonlinear flow pattern in the leeward region. The success of this approach is ascribed to solving the conservation-law form of the governing equations. The internal crossflow shock is then automatically captured to within a few mesh intervals. Improved accuracy is obtained by treating the peripheral bow shock as a sharp discontinuity forming the outer boundary of the computational domain but the captured vortical singularity remains difficult to resolve. Furthermore, the ability to capture the internal shock is bounded by an upper limit on the range of parameters $\alpha/\theta_c$ and $M_\infty$ beyond which the growing strength of the crossflow

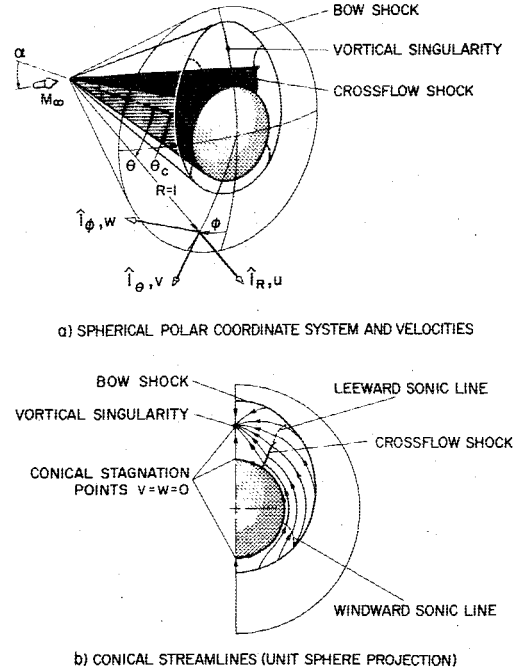


**Fig. 1 Supersonic flow about a circular cone at large angle of attack, $\alpha/\theta_c > 1$.**

Presented as Paper 77-86 at the AIAA 15th Aerospace Sciences Meeting, Los Angeles, Calif., Jan. 24-26, 1977; submitted May 23, 1977; revision received Nov. 28, 1977. 

Index categories: Supersonic and Hypersonic Flow; Shock Waves and Detonations; LV/M Aerodynamics.

*Research Assistant, Department of Aerospace Engineering, Iowa State University and Computational Fluid Dynamics Branch, NASA Ames Research Center. Member AIAA. Presently Visiting Scientist, ICASE (Institute for Computer Applications in Science and Engineering), NASA Langley Research Center, Hampton, Va.

†Research Scientist, Computational Fluid Dynamics Branch, NASA Ames Research Center. Associate Fellow AIAA.

‡Professor, Department of Aerospace Engineering, Iowa State University. Member AIAA.

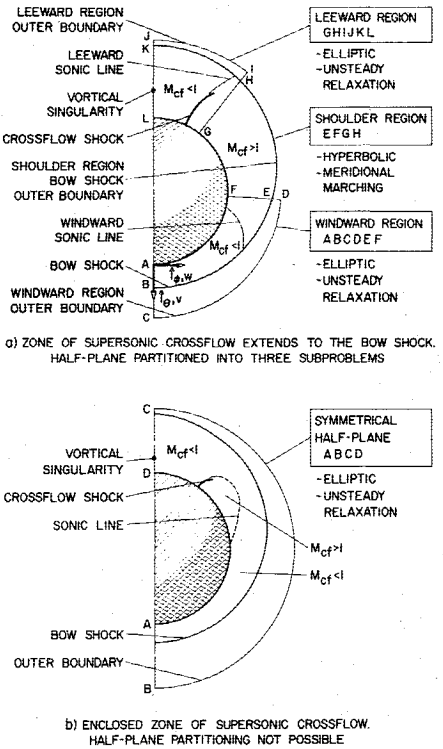


**Fig. 2 Numerical approach determined by the extent of the zone of supersonic crossflow, $M_{cf} = [(v^2 + w^2)/a^2]^{1/2}$.**

shock leads to negative pressures due to the magnitude of preshock oscillations in the captured weak solution. This range has recently been extended by altering the circular shape of the cone on the leeward side[12] or through stress terms added to the governing equations.[12,13] The resulting solutions, however, no longer represent the inviscid cone flowfield.

In contrast to the finite-difference approach, a modification of the method of lines[6,7] has been used to solve the leeward flow region provided the windward and leeward crossflow sonic lines extend to the bow shock (Fig. 2a). The method iterates on the internal shock location but utilizes a bow shock shape extrapolated from the shoulder region. The solutions obtained have been the most extensive to date, particularly in regard to the vortical singularity. The accuracy of the procedure is difficult to assess since there is considerable disagreement with the shock-captured finite-difference results. In addition, it is expected that at large angles of attack the possible nonmonotonic shape of the bow shock[14] (the maximum shock standoff distance occurring away from the leeward symmetry plane) and its vanishingly weak strength will dictate a more accurate shock boundary treatment.

This paper describes a numerical method that applies the concept of floating shock fitting[15-17] to the cone at large incidence problem. The bow shock, the embedded crossflow shock, and the vortical singularity are treated as sharp discontinuities that float simultaneously through the computational mesh. Use is made of the conservation-law form of the governing equations to aid in the detection and monitoring of the shocks. The fitting of the crossflow shock avoids the stability problems encountered with the shock-capturing approach. Furthermore, in contrast to the numerical method of Ref. 6, shock layers with limited zones of supersonic crossflow adjacent to the cone surface (Fig. 2b) can be computed. The present method is formulated to be applicable over the complete range of parameters $M_\infty$, $\alpha$, and $\theta_c$ for which the flow remains conical (bow shock wave attached).

Along with the floating-fitting method, a technique (analogous to that described in Ref. 11) in which the bow shock forms a boundary of the computational mesh has been developed. Aside from serving as a check on the floating-fitting approach, this "shock-as-a-boundary" code provides a convenient means of supplying initial conditions for the floating algorithm.

Several boundary-condition schemes have been tested in conjunction with the floating-fitting approach. Comparisons of these floating-fitting solutions with shock-as-a-boundary results are presented together with other numerical results[6,11,18] and experimental measurements.[19]

## Governing Equations—Choice of Variables

The selection of appropriate dependent and independent variables can simplify the numerical approach and result in improved accuracy. Several forms of the governing equations, each chosen with regard to its application and the flow region being computed, are used in the cone at angle of attack problem.

The general, unsteady, three-dimensional Euler equations in spherical polar coordinates (Fig. 1a) may be arranged into weak conservation-law form as

$$\tilde{U}_t + \tilde{E}_R + \tilde{F}_\theta + \tilde{G}_\phi + \tilde{H} = 0 \tag{1}$$

where $\tilde{U}$, $\tilde{E}$, $\tilde{F}$, $\tilde{G}$, and $\tilde{H}$ are five-component vectors with $\tilde{U} = \{\rho,\ \rho u,\ \rho v,\ \rho w,\ e\}^T$. For an ideal gas, the system is completed using the equation of state to relate the total energy per unit volume $e$ to the pressure $p$, density $\rho$, and velocity components $u$, $v$, and $w$ by

$$e = p/(\gamma - 1) + \rho(u^2 + v^2 + w^2)/2 \tag{2}$$

where $p$ and $\rho$ are referenced to freestream static conditions. The velocity components are normalized by $a_\infty/\sqrt{\gamma}$, where $a_\infty$ is the freestream speed of sound.

If the flowfield is assumed to be conical ($\tilde{E}_R = 0$) and steady ($\tilde{U}_t = 0$), the governing equation on the self-similar crossflow surface ($R = 1$) becomes

$$\tilde{F}_\theta + \tilde{G}_\phi + \tilde{H} = 0 \tag{3}$$

Equation (3) is elliptic for cones at small or moderate angles of attack. With increasing incidence, a small zone of supersonic crossflow forms adjacent to the body surface on the side of the cone (Fig. 2b). At still larger angles of attack, the region of supersonic crossflow extends to the bow shock. This enables partitioning of the crossflow surface into windward and leeward elliptic regions separated by the hyperbolic shoulder region (Fig. 2a).

In the application of the floating-fitting method, Eq. (3) is rendered hyperbolic by the addition of the unsteady derivative term. Alternatively, in the algorithm that fits the bow shock as a boundary, the radially asymptotic approach (addition of the conical derivative term) is followed. The unsteady approach is preferred since the hyperbolic nature is preserved for radially subsonic flows ($u < a$, where $a$ is the local speed of sound) that can occur at large angles of attack.[5]

An a priori assumption (based on previously obtained solutions) can often be made regarding the size of the region of supersonic crossflow. When partitioning is possible, maximum efficiency is achieved by solving each region separately. This frees the leeward region from the small step size imposed by the stability condition in the windward symmetry plane. In addition, a substantial part of the shoulder region can be computed in one less dimension by a $\phi$ direction marching code that integrates Eq. (3). The shoulder region algorithm (described in Ref. 1) starts from the windward region outflow boundary (with $w > a$) and sweeps around the cone until the meridional Mach number approaches unity.

The floating-fitting procedure utilizes a fixed reference mesh defined by meridional boundaries $\phi$ = constant, and a

**Table 1 Discontinuity alignment transformations**

| Coordinate system | $\theta$ direction | $\phi$ direction |
|---|---|---|
| Reference mesh | $X=\dfrac{\theta-\theta_c}{\theta_0-\theta_c}$ | $Y=\phi$ |
| Bow shock, high pressure side[a] | $X_1=\dfrac{\theta-\theta_c}{\theta_s-\theta_c}$ | $Y_1=Y$ |
| Crossflow shock, low pressure side[b,c] | $X_2=X$ | $Y_2=\dfrac{\phi-\phi_L}{\phi_{\bar{s}}-\phi_L}$ |
| Crossflow shock, high pressure side[b,c] | $X_3=X$ | $Y_3=\dfrac{\phi-\phi_u}{\phi_u-\phi_{\bar{s}}}$ |
| Vortical singularity, bow shock side[d] | $X_4=\dfrac{\theta-\theta_0}{\theta_0-\theta_{vs}}$ | $Y_4=Y$ |
| Vortical singularity, body side[d] | $X_5=\dfrac{\theta-\theta_c}{\theta_{vs}-\theta_c}$ | $Y_5=Y$ |

[a] $\theta_s=\theta_s(\phi,t)$ ~ bow shock shape. [b] $\phi_{\bar{s}}=\phi_{\bar{s}}(\theta,t)$ ~ crossflow shock shape. [c] $\phi_L,\phi_u$ ~ lower and upper meridional boundaries. [d] $\theta_{vs}=\theta_{vs}(t)$ ~ vortical singularity position.

circular outer boundary $\theta=\theta_0$. An independent variable transformation

$$X=(\theta-\theta_c)/(\theta_0-\theta_c) \qquad Y=\phi \qquad \tau=t \tag{4}$$

normalizes the cone-to-outer-boundary distance. The reference mesh for the leeward region calculation is illustrated in Fig. 3. A further transformation[20] $(\bar{X},\bar{Y},\bar{\tau})$, which permits clustering points near the cone surface and about a chosen meridional location, is used to concentrate points near the crossflow shock. Clustering is also useful in keeping the number of reference mesh points that lie outside of the shock layer (where no calculations take place) to a minimum. This is especially important when solving the symmetrical half-plane (Fig. 2b), since the bow shock is often far from being circular.

The floating-fitting technique also employs discontinuity-oriented coordinate systems, each normalizing the distance between a fixed boundary and a moving discontinuity (Fig. 3). The necessary transformations are presented in Table 1.

The governing equations are integrated on one side of each discontinuity. This integration, and the application of boundary conditions, is simplified if the nonconservative variables are used. The form of the Euler equations suitable for all discontinuity alignment transformations on the unit sphere is

$$d_\tau+[\bar{B}_1]d_{\bar{X}}+[\bar{B}_2]d_{\bar{Y}}+A_3=0 \tag{5}$$

with

$$d=\{p,u,v,w,e\}^T$$

$$[\bar{B}_1]=\{X_\theta[A_1]+X_\phi[A_2]+X_t[I]\}\bar{X}_X$$

$$[\bar{B}_2]=\{Y_\theta[A_1]+Y_\phi[A_2]+Y_t[I]\}\bar{Y}_Y$$

where $[I]$ is the identity matrix.

The derivatives of the reference mesh independent variables are evaluated for each alignment transformation $i=1,2,3,4,5$ (Table 1) where

$$X_\phi=X_\theta\theta_{X_i}X_{i_\phi}$$

$$X_t=X_\theta\theta_{X_t}X_{i_t}$$

$$Y_\theta=Y_\phi\phi_{Y_i}Y_{i_\theta}$$

$$Y_t=Y_\phi\phi_{Y_i}Y_{i_t} \tag{6}$$

with $X_\theta=1/(\theta_0-\theta_c)$ and $Y_\phi=1$.

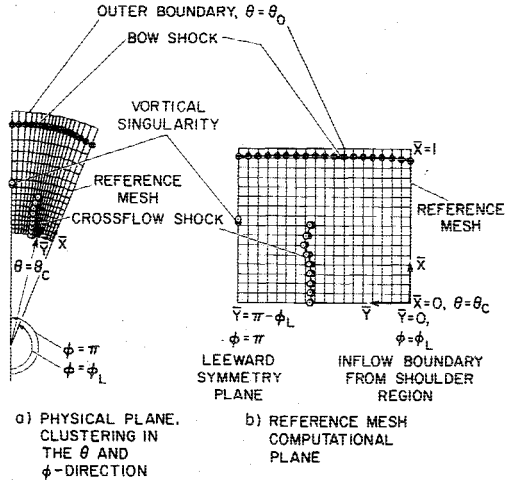


**Fig. 3 Floating discontinuities in the leeward region reference mesh.**

The choice of circular geometry for the reference mesh is responsible for the simple scaling that relates derivatives along discontinuities and derivatives in the discontinuity normalized direction to the reference mesh system. Each discontinuity mesh thus consists solely of points lying on the discontinuity while being tracked along one of the reference mesh directions (Fig. 3).

## Integration Algorithm

MacCormack's second-order, noncentered, predictor-corrector algorithm[21] is used to advance the flowfield in the time-asymptotic relaxation process. The scheme is modified for mesh points that lie on the boundaries and floating discontinuities and for points neighboring (in time or space) the floating discontinuities. In the reference mesh interior, the forward-predictor, backward-corrector sequence is followed provided the computational molecule is not crossed by a discontinuity.

In the unsteady analysis, the total enthalpy (which should equal that of the freestream in the converged solution) serves as a convenient measure of accuracy and is also used to verify the asymptotic approach to a steady state.

## Stability Analysis

Although a two-dimensional analysis is appropriate, one-dimensional amplification matrix theory yields a larger, yet stable, estimate for the step size. The influence of the discontinuity alignment transformations is reflected by the derivatives of $X$ and $Y$ appearing in the *C-F-L* condition

$$\Delta\bar{\tau}=\min(\Delta\bar{\tau}_{\bar{X}},\Delta\bar{\tau}_{\bar{Y}}) \tag{7}$$

where

$$\Delta\bar{\tau}_{\bar{X}}=\frac{(CN)\,\Delta\bar{X}}{|\sigma_{\max}([\bar{B}_1])|} \qquad \Delta\bar{\tau}_{\bar{Y}}=\frac{(CN)\,\Delta\bar{Y}}{|\sigma_{\max}([\bar{B}_2])|}$$

with

$$|\sigma_{\max}([\bar{B}_1])|=\max|\sigma([\bar{B}_1])|_i$$

$$|\sigma_{\max}([\bar{B}_2])|=\max|\sigma([\bar{B}_2])|_i$$

where $i=1,2,3,4,5$ (Table 1), and with the projections of the characteristic slopes (eigenvalues) determined by

$$|\sigma([\bar{B}_1])|=\bar{X}_X\left[\left|X_\theta v+\frac{X_\phi w}{\sin\theta}+X_t\right|+a\sqrt{X_\theta^2+\left(\frac{X_\phi}{\sin\theta}\right)^2}\right]$$

$$|\sigma([\bar{B}_2])|=\bar{Y}_Y\left[\left|Y_\theta v+\frac{Y_\phi w}{\sin\theta}+Y_t\right|+a\sqrt{Y_\theta^2+\left(\frac{Y_\phi}{\sin\theta}\right)^2}\right]$$

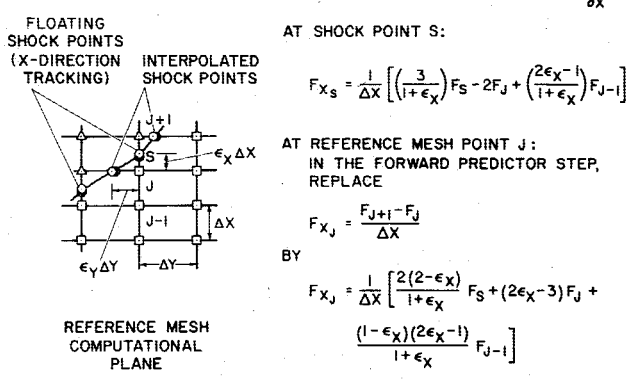


**Fig. 4 Spatial differencing approximations for floating-fitting.**

For a typical calculation the Courant parameter $CN$ is set to 0.9.

## Special Discretization Formulas

### Reference Mesh Points

Forming temporal or spatial derivative approximations using mesh points lying on opposite sides of a discontinuity is not permitted. Instead, special approximations,[17] formulated to maintain stability and accuracy, replace these differences.

*Temporal Derivatives*

The floating-fitting algorithm keeps track of the location of moving discontinuities relative to the fixed reference mesh. Movement of discontinuities over reference mesh points generally occurs only during the early transient phase. Consider the integration of

$$U_\tau + F_X + G_Y + H = 0 \tag{8}$$

where

$$U=\tilde{U} \qquad F=\tilde{F}/(\theta_0-\theta_c) \qquad G=\tilde{G} \qquad H=\tilde{H}$$

using MacCormack's scheme. Referring to Fig. 4, if the shock point $S$ is located between reference mesh points $J$ and $J-1$ at time level $n$ and crosses point $J$ (moving in the $X$ direction) while advancing to time level $n+1$, then $U_J^{n+1}$ is computed by the linear interpolation

$$\overline{U_J^{n+1}} = (\overline{U_S^{n+1}} + \epsilon_X \overline{U_{J-1}^{n+1}})/(1+\epsilon_X) \tag{9}$$

*Spatial Derivatives*

The replacement of reference mesh spatial derivatives in MacCormack's scheme is illustrated in Fig. 4. The approximation§ shown for $F_{X_J}$ was found to yield results equivalent to those obtained using a formula that involved an additional point in the reference mesh.[15] The removal of even one point offers coding simplification.

If the shock in Fig. 4 also cuts the mesh interval $J$ to $J-1$ so that $F_{J-1}$ is not available for the computation of $F_{X_J}$, then $F_{X_J}$ is approximated by

$$F_{X_J} = (F_S - F_{SL})/(X_S - X_{SL}) \tag{10}$$

where $S$ and $SL$ represent shock points lying above and below the reference mesh point $J$.

If point $J$ is on an $X$ boundary, so that no points are below it, then $F_{X_J}$ is computed using

$$F_{X_J} = (F_S - F_J)/(\epsilon_X \Delta X) \quad \text{for } \epsilon_X \geq \tfrac{1}{2} \tag{11}$$

§The authors wish to thank Manuel Salas of NASA Langley Research Center for providing this formula.

for $\epsilon_X < \frac{1}{2}$, $F_{X_J}$ is obtained by extrapolation of $F_X$ in the $Y$ direction.

Similar discretization formulas apply to the required $Y$ derivatives at point $J$. However, since shock values are tracked along $Y=$ constant lines (for the example shown in Fig. 4), interpolation is required to obtain $G_S$ values where the shock cuts a $\Delta Y$ mesh interval. Linear interpolation has been found to be sufficient.

### Discontinuity Mesh Points

Derivatives along the shock in Fig. 4 are computed using the usual MacCormack scheme. Derivatives in the shock-normalized direction, obtainable in terms of $X$ derivatives, are computed using the $F_{X_S}$ equation[17] shown in Fig. 4.

The same derivative approximations are used at the crossflow shock and at the bow shock, except that the roles of $X$ and $Y$ are interchanged. Bow shock points are tracked in the $X$ direction while crossflow shock points move in the $Y$ direction.

$X$ derivatives at the vortical singularity are similar to those at bow shock points since the vortical singularity is also tracked in the $X$ direction. For the $Y$ derivative at the vortical singularity ($w_Y$ being the only nonzero $Y$ derivative), interpolated reference mesh values must be used.

## Initial Conditions

Freestream conditions or very approximate initial guesses are often sufficient to initiate a shock-capturing relaxation procedure. Somewhat more care is required in specifying the initial flowfield when a peripheral shock is treated as an outer boundary. If all discontinuities are to be fitted, the determination of initial conditions can become very involved. In the case of a cone at large angle of attack, the problem is further complicated by the difficulty of obtaining a physically relevant flowfield that can evolve into the desired conical flow. For many cases of interest, the idea of starting with a sphere-cone solution is ruled out by the failure of existing sphere-cone codes at large angles of attack. At smaller angles of attack, where solutions can be obtained, the presence of strong entropy gradients from the blunt nose may require special treatment.

The initialization procedure for the floating-fitting algorithm is detailed in Ref. 1. Essentially, the strategy is to start from a flowfield obtained by choosing shock shape and surface distribution parameters or by using previously computed solutions with nearly the same values of $M_\infty$, $\theta_c$, and $\alpha$. This starting flow is then further refined by iteration with the code that fits the bow shock as a boundary and captures embedded discontinuities. Only a few iterations are required to establish a flowfield that is suitable for the floating-fitting technique to adequately detect the forming embedded discontinuities. Instabilities that may arise with the capturing code, if strong crossflow shocks are present, are avoided by beginning the floating-fitting technique in the early stages of shock formation.

## Boundary Conditions

### One-Sided Differencing

The implementation of boundary condition schemes at reference mesh points on the cone surface and the symmetry plane involves the evaluation of derivatives normal to these surfaces. Similarly, at floating mesh points on each side of the discontinuity, derivatives in the discontinuity-normalized direction are required. At reference mesh points, equally spaced, three-point, one-sided approximations are used in both the predictor and corrector steps of MacCormack's algorithm, provided a discontinuity is not encountered. Suitable one-sided approximations for reference mesh points in the vicinity of discontinuities, and for floating mesh points, have been given in the Special Discretization Formulas section of this paper.

**Cone Surface**

The shock-as-a-boundary code employs Abbett's[22] Euler predictor/simple-wave corrector procedure at the cone surface. The application of the method parallels the steps outlined in Ref. 11.

The floating-fitting code uses Kentzer's[23] impermeable wall scheme. Also included in the floating-fitting code is a simple scheme which overwrites flow values obtained from one-sided differencing by imposing tangency and entropy conditions (as described in Ref. 1).

Kentzer's approach combines the differentiated surface tangency condition ($v_{\bar{\tau}}=0$) with the compatibility relation along the down-running characteristic in the $\bar{X}$, $\bar{\tau}$-plane, resulting in a differential equation for the surface pressure

$$p_{\bar{\tau}}=(ap_{\bar{X}}-\gamma pv_{\bar{X}})\frac{\bar{X}_X}{\theta_0-\theta_c}-(wp_{\bar{Y}}+\gamma pw_{\bar{Y}})\frac{\bar{Y}_Y}{\sin\theta_c}$$

$$-a\rho(2au+w^2\cot\theta_c) \tag{12}$$

With $v=0$, the remaining velocity components $u$ and $w$ are computed using, respectively, the $R$- and $\phi$-momentum equations, the second and fourth rows of Eq. (5).

Derivatives along the cone surface ($\bar{Y}$ direction) are approximated by the MacCormack forward-backward sequence, or, if neighboring a discontinuity, by the special discretization formulas. The only exception is the $w_{\bar{Y}}$ derivative in the $\phi$-momentum equation, which is always approximated by backward differences.

As part of the relaxation process, the entropy along the body at the new time level is determined by first advancing the bow shock in the windward symmetry plane (not required if solving only the leeward region) and the crossflow shock at the body surface. These updated entropy values are imposed on the body upstream and downstream of the crossflow shock at its new location. With entropy $S$, velocities, and pressure known, density follows from

$$\rho=(p/S)^{1/\gamma} \tag{13}$$

and $e$ from Eq. (2).

**Inflow and Outflow Meridional Boundaries**

The three subproblems making up the partitioned half-plane (Fig. 2a) are joined by meridional inflow and outflow boundaries.

In the windward region the outflow boundary must be selected such that it lies beyond the limiting characteristic in the crossflow plane. Simple extrapolation then provides flow values for this supersonic outflow boundary.

The shoulder region $\phi$ marching code obtains initial data from the converged windward solution. The $w$ velocity must be supersonic all along the initial data line. The $\phi$ direction sweep around the cone is terminated when the $w$ velocity drops to sonic speed. In practice, a cutoff of $w=1.05a$ is used since the $\phi$ step size approaches zero as $w$ approaches $a$.

The leeward region inflow boundary values are held fixed at values determined from the shoulder region code.

**Discontinuities**

The shock-as-a-boundary procedure uses Thomas'[20] "pressure approach" for propagating the bow shock. Its adaptation to the shoulder region calculation is presented in Ref. 1. In the windward, leeward, and symmetrical half-plane problems, the use of Thomas' scheme is similar to the application discussed in Ref. 11.

The floating-fitting technique utilizes Kentzer's approach, which is based on the theory of characteristics, to move the bow shock, embedded crossflow shock, and the vortical singularity.

*Detection and Monitoring*

Embedded discontinuities are searched for in the flowfield provided by the initial conditions. The vortical singularity is located at the maximum density gradient in the leeward symmetry plane.

Crossflow shock points are located by continually scanning the pressure distribution along $\theta=$ constant lines. Trial shock points are positioned at the maximum compressive gradient (as computed by the conservation-law form of the governing equations). A normal Mach number is computed with extrapolated upstream flow values and a finite-difference approximation for the shock slope. If the normal Mach number is greater than one, then tracking of the trail shock point as a shock point begins.

A check for embedded shock points is made after each advancement, with points being added or discarded. The embedded shock forms early and locks into place near the cone surface. However, the end-point of the embedded shock tends to oscillate. To eliminate this problem without the complications of treating the true shock tip, an artificial cutoff of the fitted shock is made. Some small overshoots and undershoots, typical of shock-captured solutions, are observed at the truncated shock tip. However, these small errors do not propagate away from the truncated shock tip.

*Propagation*

Following Kentzer's[23] approach, a characteristic compatibility relation is combined with the differentiated discontinuity jump conditions to yield an equation for the acceleration of the discontinuity. The updated discontinuity speed and position are obtained by integrating the acceleration using a second-order Euler predictor/modified Euler corrector method.

The updated flow values on one side of the discontinuity are obtained by integrating the nonconservative form of the discontinuity aligned governing equations [Eq. (5)], with the exception of the bow shock where one side is the known freestream. At the crossflow shock, the governing equations are integrated on the low pressure (crossflow upstream) side. At the vortical singularity, the integration is performed on the low entropy (bow shock) side.

With the updated geometry and flow values known on one side, the updated flow values on the opposite side of the discontinuity are determined by the jump conditions.

The implementation of Kentzer's scheme may be illustrated by considering the propagation of the crossflow shock. Crossflow shock points are tracked in the $\bar{Y}$ direction. Using the notation and definitions shown in Fig. 5, $q_{\bar{S}_{\bar{\tau}}}$ represents the acceleration of the crossflow shock, normal to the shock and pointing toward the high pressure side. The equation for the crossflow shock acceleration (with clustering in the reference mesh) obtained by combining the compatibility relation along the down-running characteristic in the $\bar{Y}_3$, $\bar{\tau}$-plane (Table 1) with the $\bar{\tau}$-differentiated Rankine-Hugoniot jump conditions, is

$$q_{\bar{S}_{\bar{\tau}}}=\tilde{R}_1(\tilde{R}_2+\tilde{R}_3+\sigma\tilde{R}_4+\tilde{R}_5+\tilde{R}_6) \tag{14}$$

where

$$\tilde{R}_1=\frac{\gamma+1}{2\left\{2\rho_1\tilde{u}_{1_{\text{rel}}}+a\rho\left[1+\left(\frac{1}{\tilde{M}_{1_{\text{rel}}}}\right)^2\right]\right\}}$$

$$\tilde{R}_2=\frac{\tilde{u}_{1_{\bar{\tau}}}}{\gamma+1}\left\{4\rho_1\tilde{u}_{1_{\text{rel}}}-a\rho\left[(\gamma-1)-2\left(\frac{1}{\tilde{M}_{1_{\text{rel}}}}\right)^2\right]\right\}$$

$$+\frac{p_{1_{\bar{\tau}}}}{\gamma+1}\left[2\gamma\tilde{M}^2_{1_{\text{rel}}}-(\gamma-1)\right]-\frac{4a_{1_{\bar{\tau}}}}{\gamma+1}\left(\rho_1\tilde{u}_{1_{\text{rel}}}\tilde{M}_{1_{\text{rel}}}+\frac{a\rho}{\tilde{M}_{1_{\text{rel}}}}\right)$$

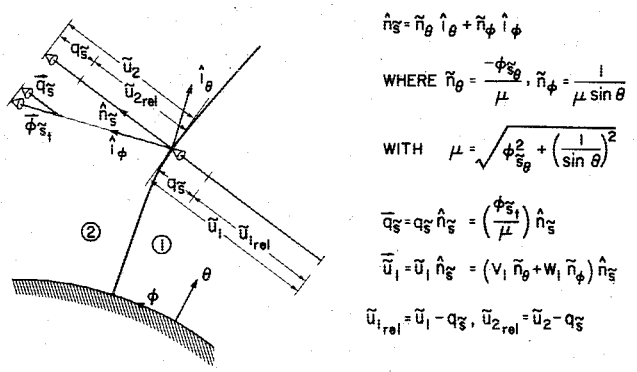


Fig. 5 Crossflow shock geometry and motion.

$$\tilde{R}_3 = a\rho(v\tilde{n}_{\theta_{\tilde{T}}} + w\tilde{n}_{\phi_{\tilde{T}}})$$

$$\tilde{R}_4 = [p_{\tilde{Y}} - a\rho(\tilde{n}_\theta v_{\tilde{Y}} + \tilde{n}_\phi w_{\tilde{Y}})]\tilde{Y}_Y$$

$$\tilde{R}_5 = \frac{1}{\theta_0 - \theta_c}\left\{(v - a\tilde{n}_\theta)p_{\tilde{X}} + a\rho[(a - v\tilde{n}_\theta)v_{\tilde{X}} - v\tilde{n}_\phi w_{\tilde{X}}]\right\}\tilde{X}_X$$

$$\tilde{R}_6 = a\rho\{a(2u + v\cot\theta) - [\tilde{n}_\theta(uv - w^2\cot\theta) + \tilde{n}_\phi w(u + v\cot\theta)]\}$$

In Eq. (14), the down-running characteristic is defined by

$$\sigma = -\phi_{\tilde{s}_\theta} v + \frac{w}{\sin\theta} - \phi_{\tilde{s}_t} - a\mu \tag{15}$$

the upstream normal relative Mach number is

$$\tilde{M}_{l_{\text{rel}}} = \tilde{u}_{l_{\text{rel}}}/a_l \tag{16}$$

and the nonsubscripted flow values represent the crossflow shock downstream conditions.

As noted, for example, in Refs. 15 and 16, shock acceleration equations can be very sensitive to the manner in which they are discretized. The crossflow shock acceleration Eq. (14) is no exception.

Following the suggestions in Ref. 15, the $\tilde{R}$ terms in Eq. (14) are grouped according to differing physical roles. The accurate calculation of $\tilde{R}_5$ requires that the $v_{\tilde{X}}$ and $w_{\tilde{X}}$ difference approximations include discontinuity mesh points that lie midway between the mesh points being tracked. The inclusion of this so-called "variable-area"[15] effect thus doubles the number of discontinuity-mesh points. The location of these intermediate mesh points is determined by the points being tracked. The evaluation of the temporal derivatives in $\tilde{R}_2$ at the intermediate mesh points introduces the further complication of obtaining upstream flow values by interpolation in the reference mesh. However, with these added mesh points the tendency of the crossflow shock to develop kinks is removed.

The propagation of the bow shock and the vortical singularity is analogous to, but much simpler than, that described for the embedded crossflow shock.

## Results

The partitioning of the crossflow surface into separate windward, shoulder, and leeward region problems (Fig. 2a) is demonstrated by solving the case: $M_\infty = 7$, $\theta_c = 20$ deg, and $\alpha = 30$ deg. Additional windward region results are obtained for the case: $M_\infty = 7.95$, $\theta_c = 10$ deg, and $\alpha = 16$ deg to compare numerical solutions with experimental measurements on the side of the cone where viscous effects are small. The symmetrical half-plane problem (Fig. 2b), where partitioning is not possible, is demonstrated by computing the case: $M_\infty = 3$, $\theta_c = 7.5$ deg, and $\alpha = 15$ deg.

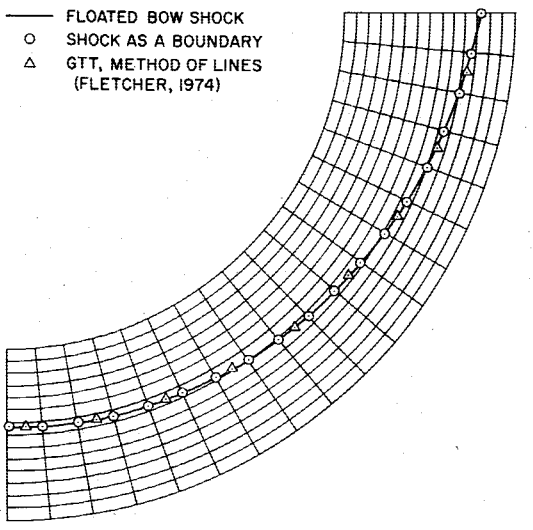


Fig. 6 Floated bow shock in the windward region reference mesh. Comparison of bow shock shapes; $M_\infty = 7$, $\theta_c = 20$ deg, $\alpha = 30$ deg.

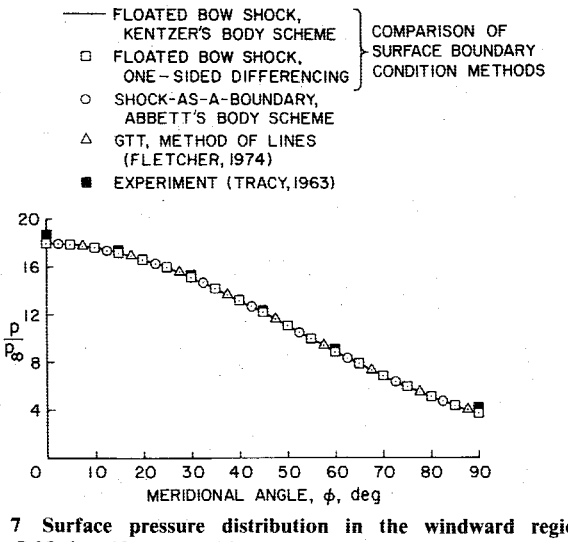


Fig. 7 Surface pressure distribution in the windward region; $M_\infty = 7.95$, $\theta_c = 10$ deg, $\alpha = 16$ deg.

Calculations of the windward region problem were obtained first to assess the stability and accuracy of the floating-fitting approach (thus avoiding the additional complexity of embedded discontinuities) and to test several boundary-condition procedures.

Figure 6 shows the solution for the floated bow-shock shape in the reference mesh compared with the shock-as-a-boundary results and a method of lines solution.[6] The methods are in excellent agreement. Numerous crossings of the reference mesh $\theta$ = constant grid lines are demonstrated to have no adverse effect on the floating-fitting results.

Body boundary-condition methods are compared in Fig. 7 for a windward region case where experimental results are also available.[19] The numerical methods all tend to produce the same result. The difference between the numerical and experimental values is probably due largely to experimental errors.[4]

In Fig. 8, the solution from the shoulder region $\phi$ marching code is shown together with the windward region results in the form of crossflow surface contour plots. The acceleration around the cone shoulder is demonstrated by the crossflow Mach number levels in Fig. 8a. The windward crossflow sonic line lies well upstream of the windward outflow boundary located at $\phi = 90$ deg. The constant entropy contours in Fig. 8b represent the streamline pattern. The shoulder region

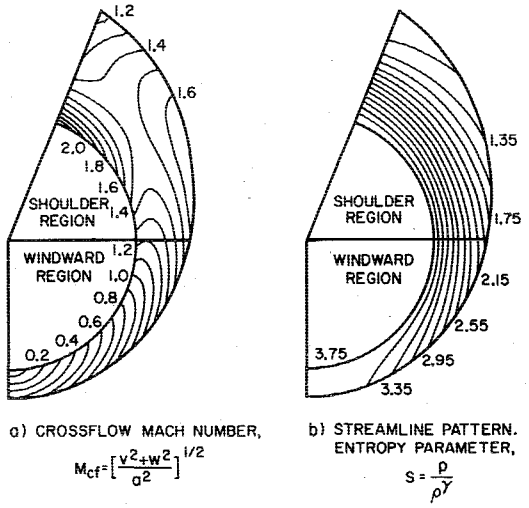


**Fig. 8 Crossflow Mach number and entropy parameter contours in the windward and shoulder regions; $M_\infty = 7$, $\theta_c = 20$ deg, $\alpha = 30$ deg.**

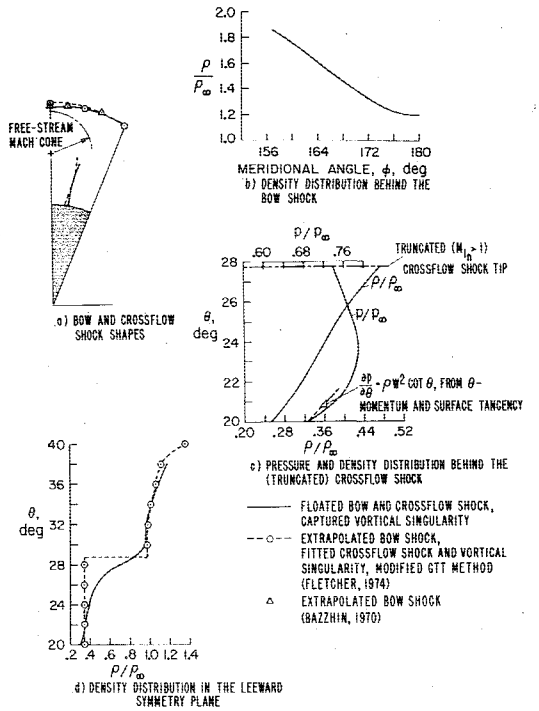


**Fig. 9 Leeward region solution; $M_\infty = 7$, $\theta_c = 20$ deg, $\alpha = 30$ deg.**

contours match precisely those obtained by the method of characteristics.[6,18]

Results for the leeward region flowfield are presented in Fig. 9. The floated bow shock dips slightly in the leeward symmetry plane (Fig. 9a). The shock shape thus represents the so-called "anomalous position"[5,14] and differs from the regular position of the extrapolated bow shock. The density distribution behind the floated bow shock is plotted in Fig. 9b.

The crossflow shock in Fig. 9a is perpendicular to the surface at its base. Away from the surface, the crossflow shock bends very slightly toward the crossflow upstream direction. The normal intersection of the crossflow shock with the cone surface is not imposed in the floating-fitting code, but evolves as the steady-state solution is approached. The length of the crossflow shock in Fig. 9a is the length of the fitted portion only. The fitting scheme is not applied all the way to the crossflow shock tip.

The pressure and density distributions on the downstream side of the crossflow shock are shown in Fig. 9c. Tentative

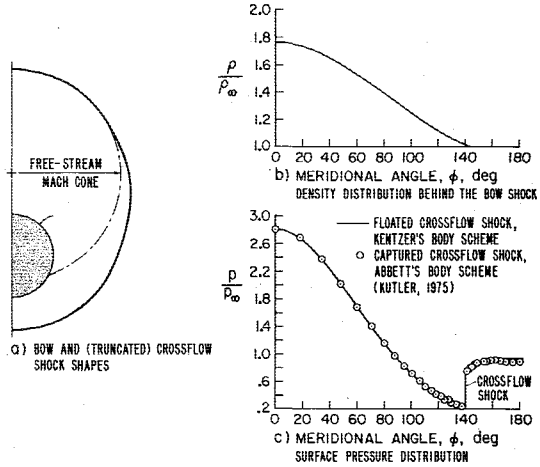


**Fig. 10 Symmetrical half-plane solution; $M_\infty = 3$, $\theta_c = 7.5$ deg, $\alpha = 15$ deg.**

evidence of the presence of a conical logarithmic singularity (analogous to that found in two-dimensional flow) is provided by noting the difference between the Rankine-Hugoniot determined $p_\theta$ slope at the cone surface with that from the normal momentum equation with $v = 0$ (plotted as a dashed line in Fig. 9c).

The leeward symmetry plane density distribution, obtained by solving the conservation-law form of the governing equations without any special treatment of the vortical singularity, is compared with a modified GTT method solution[6] in Fig. 9d. The density jump is spread out over several $\theta$ degrees. It may be inferred from the leeward symmetry plane density and $u$ velocity distributions that liftoff of the vortical singularity has occurred. Liftoff, however, is not verified by the leeward symmetry plane, $v$ velocity distribution. Floating-fitting a trial vortical singularity, positioned initially at the maximum density gradient, does not alter the sign of the $v$ velocity. This result may be due to the use of the conservation-law form of the equations in the flowfield interior that smooths out the sharp density gradients in meridional planes near the plane of symmetry. A new set of dependent variables (similar to those suggested in Ref. 24) might help to resolve the singularity. However, the conservation-law form has proven to be very convenient with regards to the crossflow shock, end-point treatment; such benefits would be lost with a change of dependent variables.

A symmetrical half-plane solution is presented in Fig. 10. The bow shock loses its strength on the leeward side as it approaches tangency with the freestream Mach cone (Fig. 10a). The density behind the bow shock, plotted in Fig. 10b, thus becomes equal to that of the freestream on the leeward side. Kentzer's shock boundary scheme accurately maintains the zero-strength shock solution.

As shown in Fig. 10a, the crossflow shock (fitted portion) does not extend very far into the flowfield interior. The pressure jump across the crossflow shock is apparent in Fig. 10c where the surface pressure distribution is shown. The floating-fitting results in Fig. 10c match those obtained by a shock-capturing approach with slight differences occurring downstream of the crossflow shock.

## Conclusions

Complicated flowfields occur about the geometrically simple circular cone at large angles of attack. Thus, the cone at large incidence serves as a model problem for more complex geometries and provides a convenient test of numerical techniques for computing multidimensional flows containing embedded discontinuities.

In this paper an explicit finite-difference technique, based on the concept of floating-fitting discontinuities, has been

described. Results have been presented that demonstrate the capability of the method over a range of Mach numbers, cone angles, and angles of attack. The technique has been shown to compute accurately both strong embedded shocks and vanishingly weak peripheral shocks. The method does not resolve the structure of the flowfield in the immediate vicinity of the vortical singularity.

The computer code for the floating-fitting algorithm, which must include logic for numerous discontinuity configurations in the computational mesh, is necessarily lengthy. However, most mesh points require no special treatment so that a typical case with 330 mesh points requires less than 15 min on an IBM 360/67 to achieve convergence.

## Acknowledgments

Funds for the support of this study have been allocated by the NASA Ames Research Center, Moffett Field, Calif., under Interchange No. NCA2-OR340-603.

## References

[1] Daywitt, J. E., "Computation of the Inviscid Supersonic Flow About Cones at Large Angles of Attack by a Floating Discontinuity Approach," Ph.D. Dissertation, Iowa State University, Ames, Iowa, 1977.

[2] Ferri, A., "Supersonic Flow Around Circular Cones at Angles of Attack," NACA Technical Note 2236, Nov. 1950.

[3] Melnik, R. E., "Vortical Singularities in Conical Flow," *AIAA Journal*, Vol. 5, April 1967, pp. 631-637.

[4] Jones, D. J., "Numerical Solutions of the Flow Field for Conical Bodies in a Supersonic Stream," National Research Council of Canada Aeronautical Report LR-507, July 1968.

[5] Bachmanova, N. S., Lapygin, V. I., and Lipnitskii, Y. M., "Supersonic Flow Past Circular Cones at Large Angles of Attack," *Fluid Dynamics*, Vol. 8, May 1975, pp. 915-919.

[6] Fletcher, C. A. J., "Supersonic Flow About Cones at Large Angles of Attack," College of Engineering Report No. FM-74-8, University of California, Berkeley, May 1974.

[7] Fletcher, C. A. J., "Vortical Singularity Behind a Highly Yawed Cone," *AIAA Journal*, Vol. 13, Aug. 1975, pp. 1073-1078.

[8] George, O. L., "An Experimental Investigation of the Flow Field Around an Inclined Sharp Cone in Hypersonic Flow," SC-RR-69-577, Sandia Laboratories, Albuquerque, New Mexico, Sept. 1969.

[9] Nebbeling, C. and Bannink, W. J., "Experimental Investigation of the Supersonic Flow Field About a Slender Cone at High Incidences," Dept. of Aerospace Engineering Report LR-233, Delft University of Technology, Delft, The Netherlands, Nov. 1976.

[10] Ivanov, M. Y. and Kraiko, A. M., "Calculation of the Supersonic Flow Around Conical Bodies," *U.S.S.R. Computational Mathematics and Mathematical Physics*, Vol. 13, Jan. 1975, pp. 228-245.

[11] Kutler, P., "Computation of Three-Dimensional, Inviscid Supersonic Flows," *Progress in Numerical Fluid Dynamics, Lecture Notes in Physics*, Vol. 41, edited by H. J. Wirz, Springer-Verlag, Berlin, 1975, pp. 287-374.

[12] Miyazawa, M., "A Numerical Analysis of Conical Flowfields," *Proceedings of the 10th International Symposium on Space Technology and Science*, Tokyo, 1973, pp. 433-442.

[13] McRae, D. S., "A Numerical Study of Supersonic Viscous Cone Flow at High Angle of Attack," AIAA Paper 76-97, Washington, D.C., 1976.

[14] Zolotova, N. V., "On the Shape of the Shock in Nonsymmetric Hypersonic Flow Around a Circular Cone," *Fluid Dynamics*, Vol. 9, June 1975, pp. 137-139.

[15] Moretti, G., "Floating Shock Fitting Technique for Imbedded Shocks in Unsteady Multidimensional Flows," *Proceedings of the 1974 Heat Transfer and Fluid Mechanics Institute*, Corvallis, Ore., June 12-14, 1974, pp. 184-201.

[16] Moretti, G., "A Circumspect Exploration of a Difficult Feature of Multidimensional Imbedded Shocks," *Proceedings of the AIAA 2nd Computational Fluid Dynamics Conference*, Hartford, Conn., June 19-20, 1975, pp. 10-16.

[17] Salas, M., "The Anatomy of Floating Shock Fitting," *Proceedings of the AIAA 2nd Computational Fluid Dynamic Conference*, Hartford, Conn., June 19-20, 1975, pp. 47-54.

[18] Bazzhin, A. P., "Some Results of Calculations of Flows Around Conical Bodies at Large Incidence Angles," *Proceedings of the Second International Conference on Numerical Methods in Fluid Dynamics, Lecture Notes in Physics*, Vol. 8, edited by M. Holt, Berkeley, Calif., Sept. 15-19, 1970, pp. 223-229.

[19] Tracy, R. R., "Hypersonic Flow over a Yawed Circular Cone," Graduate Aeronautical Laboratories Memorandum No. 69, California Institute of Technology, August 1963.

[20] Thomas, P. D., Vinokur, M., Bastianon, R., and Conti, R. J., "Numerical Solution for the Three-Dimensional Hypersonic Flow Field of a Blunt Delta Body," *AIAA Journal*, Vol. 10, July 1972, pp. 887-894.

[21] MacCormack, R. W., "The Effect of Viscosity in Hypervelocity Impact Cratering," AIAA Paper 69-354, Cincinnati, Ohio, 1969.

[22] Abbett, M. J., "Boundary Condition Computational Procedures for Inviscid Supersonic Steady Flow Field Calculations," Final Report No. 71-41, Aerotherm Corporation, 1971.

[23] Kentzer, C. P., "Discretization of Boundary Conditions on Moving Discontinuities," *Proceedings of the Second International Conference on Numerical Methods in Fluid Dynamics, Lecture Notes in Physics*, Vol. 8, edited by M. Holt, Berkeley, Calif., Sept. 15-19, 1970, pp. 108-113.

[24] Pandolfi, M., "Supersonic Flow About Elliptic Cones with Large Semiaxis Ratios," Pubblicazione N. PP172, Instituto Di Macchine E Motori Per Aeromobili, Dec. 1975.